

Reduced fractional absorption and second harmonic emission in laser-produced plasmas

H. Ruhl^{a)}

Theoretische Quantenelektronik, TH-Darmstadt, Hochschulstrasse 4A, 64289 Darmstadt, Germany

R. A. Cairns

School of Mathematical and Computational Sciences, University of St. Andrews, North Haugh, St. Andrews, Fife, KY1 9SS, United Kingdom

(Received 1 October 1996; accepted 4 March 1997)

Both particle-in-cell and Vlasov simulations of the collective absorption of p -polarized intense laser light incident on a plasma with a steep density profile show the fractional absorption decreasing with intensity for large angles of incidence. Here an analytical model is developed that indicates that this effect for a high-temperature plasma ($T_e \geq 2.5$ keV) is connected with the conversion of a large fraction of the incident energy into harmonic emission. Good agreement between the results of Vlasov simulations and those of the nonlinear analytical model are obtained. © 1997 American Institute of Physics. [S1070-664X(97)01206-8]

I. INTRODUCTION

Terrawatt laser systems have created novel experimental conditions in which it is possible to produce near solid density plasmas, with density scale lengths at the boundary a fraction of the vacuum wavelength. Experiments with s - and p -polarized light have shown that absorption is enhanced for the latter, indicating that a substantial fraction of the absorption is purely collective.^{1,2} Recent experiments and theory^{3,4} support this conclusion and suggest that at irradiances $I\lambda^2 \geq 10^{17}$ W cm⁻² μm² pulses with no prepulse enter a universal regime of an ideal plasma interacting with laser light. Simulations performed by Gibbon *et al.*⁵⁻⁷ and by Ruhl⁸ predict that fractional absorption of ultrashort laser pulses by purely collective effects decreases with growing irradiance.

In this paper we aim to explain this effect by a self-consistent analytic kinetic approach. We will link it to enhanced emission of the second harmonic in the limit of high temperatures. We will see that dominant terms involve the electric field perpendicular to the interface as was found recently by Yang *et al.*⁹ and previously by the author.¹⁰

The reason for the electric field perpendicular to the interface playing the dominant role for harmonic emission has a simple physical explanation as follows. If the normal to the interface is in the x direction, the electrostatic component of the force normal to the interface is to leading order,

$$\langle \rho E_x \rangle = \frac{\epsilon_0}{2} \partial_x \langle E_x^2 \rangle. \quad (1)$$

Taking the positive direction to be from the medium to the vacuum, this force acts toward the vacuum. There is also, of course, the $\mathbf{j} \times \mathbf{B}$ force. If we neglect the displacement current the magnetic force is (the incident wave being taken to be polarized with its electric field in the x - y plane)

$$\langle j_y B_z \rangle = -\frac{c^2 \epsilon_0}{2} \partial_x \langle B_z^2 \rangle. \quad (2)$$

This force acts inward and, when integrated through the skin layer, gives a total force greater than the electrostatic component, so the total radiation pressure on the plasma is inward, as would be expected. One of the crucial features of the plasma response for our present work is that there are two separate skin lengths and that the longitudinal electric field produced by charge separation at the surface decays more rapidly than the electromagnetic field. This means that the outward component of the force described above is dominant near the surface, while the force on the electrons farther into the plasma is negative. This explains the surface layer of enhanced electron density seen in simulations.^{6,8} Also, the large electron density perturbation in the longitudinal skin layer produces the dominant term in the second-order current for the steep density profiles considered.

In Sec. II we will give a detailed derivation of the analytical plasma model and describe the approximations made. In Sec. III we will give an approximate solution of the equations of Sec. II. Ultimately, in Sec. V we will compare the results of the analytical model with fully nonlinear Vlasov calculations.

II. MODEL EQUATIONS

We now give an analytic estimate of the plasma response that will justify the above remarks. The analytical solution given in Sec. III will provide an estimate of the second harmonic emission over a large range of parameters. Use is made of the well-known boosting technique,¹¹ which yields an additional constant of motion. The boosted frame will be used throughout this paper. For the initial electron distribution a Maxwellian is taken. A step-like density profile for the electrons with $n(x) = n_0$ for $x > 0$ is assumed. We then obtain for the electron distribution at arbitrary times,

$$f(t) = \frac{n_0}{\sqrt{2\pi^3 m^3 v_{th}^3}} \exp\left(-\frac{p_x^2(0) + p_z^2(0)}{2m^2 v_{th}^2}\right) \times \exp\left(-\frac{(p_y(0) + \bar{\beta} \bar{\gamma} m c)^2}{2\bar{\gamma}^2 m^2 v_{th}^2}\right), \quad (3)$$

^{a)}Electronic mail: Hartmut.Ruhl@physik.th-darmstadt.de

where

$$x(\tau) = x - \int_{\tau}^t d\eta v_x(\eta),$$

$$p_x(\tau) = p_x + e \int_{\tau}^t d\eta \{E_x[x(\eta), \eta] + v_y(\eta) \partial_x A_y[x(\eta), \eta]\},$$

$$p_y(\tau) = p_y + e[A_y(x(\tau), \tau) - A_y(x, t)],$$

$$p_z(\tau) = p_z. \quad (4)$$

The quantities $\bar{\beta}$ and $\bar{\gamma}$ are given by $\bar{\beta} = \sin \theta$ and $\bar{\gamma} = 1/\sqrt{1-\bar{\beta}^2}$, where θ denotes the angle of incidence.

We will approximate the first of the Eqs. (4) by $x(\tau) = |x - v_x(t - \tau)|$. We would like to note that different approximations for this equations naturally lead to the various collective absorption mechanisms discussed in the literature.^{4,9,12} A detailed summary of these is found in the paper by Rozmus *et al.*⁴ The straight line approximation certainly becomes invalid as soon as large numbers of electrons are allowed to penetrate into the vacuum.¹² We will see by comparison with fully nonlinear Vlasov simulations to what extent the straight line approximation is justified (see Sec. IV).

We next expand the electron distribution function and keep only those terms that are at most quadratic in the field amplitudes. On a formal mathematical basis such an expansion is valid if $\omega_p v_{os}^2 / \omega c v_{th} < 1$. In deriving this condition we assumed that field amplitudes in the plasma are of the order of the vacuum amplitudes. This assumption overestimates the field strengths. We shall see later by comparing the results of the analytical model with Vlasov simulations to what extent this restriction can be relaxed. The parameter indicates that high temperatures tend to linearize the interaction of the laser pulse with the plasma.

In a second step the charge and current densities ρ , j_x , and j_y are calculated, with the help of the approximation obtained for f and introduced into Maxwell's equations, giving

$$\begin{aligned} \partial_x E_x \approx & \frac{\omega_p^2 \bar{\gamma}}{\sqrt{2} \pi v_{th}} \int_{-\infty}^{\infty} dp_x \frac{p_x}{m^2 v_{th}^2} e^{-p_x^2/2m^2 v_{th}^2} \\ & \times \int_0^t d\tau \left(E_x^L + \frac{e A_y \partial_x A_y}{m \bar{\gamma}^3} \right), \end{aligned} \quad (5)$$

$$\begin{aligned} \partial_t E_x \approx & - \frac{\omega_p^2 \bar{\gamma}}{\sqrt{2} \pi v_{th}} \int_{-\infty}^{\infty} dp_x \frac{p_x^2}{m^3 v_{th}^2 \bar{\gamma}} e^{-p_x^2/2m^2 v_{th}^2} \\ & \times \int_0^t d\tau \left(E_x^L + \frac{e A_y \partial_x A_y}{m \bar{\gamma}^3} \right), \end{aligned} \quad (6)$$

and

$$\begin{aligned} \left(\partial_x^2 - \frac{1}{c^2} \partial_t^2 \right) A_y \approx & \frac{\omega_p^2 \bar{\gamma}}{\sqrt{2} \pi v_{th} c^2} \int_{-\infty}^{\infty} dp_x e^{-p_x^2/2m^2 v_{th}^2} \\ & \times \int_0^t d\tau \left[\frac{1}{m \bar{\gamma}^3} \partial_{\tau} A_y + \frac{p_x}{m^2 v_{th}^2} \left(\bar{\beta} c E_x^L \right. \right. \\ & \left. \left. - \frac{e A_y(t) E_x^L}{m \bar{\gamma}^3} + \bar{\beta} c \frac{e A_y \partial_x A_y}{m \bar{\gamma}^3} \right) \right], \end{aligned} \quad (7)$$

where $E_x^L = E_x - \bar{\beta} c \partial_x A_y$. We would like to note that Eqs. (5), (6), and (7) are of nonlocal nature. The term proportional to E_x^L describes the zeroth-order coupling of the transverse field A_y to the electrostatic field. This coupling leads to Fresnel-type formulas for fractional absorption, as given by Andreev *et al.*¹³ In addition, we have a second-order coupling term, $A_y(t) E_x^L$, which describes the coupling of the transverse field to longitudinal plasma oscillations. These surface oscillations show up as the oscillating electrostatic field E_x^L . The oscillation amplitude is of the order of a Debye length. The relevance of this effect for harmonic generation has been suggested by Erokhin *et al.*¹⁴ and recently by Lichters *et al.*¹⁵ The other second-order term given by $A_y \partial_x A_y$ describes the self-coupling of the transverse field in the skin layer.

The quadratic terms in Eqs. (5), (6), and (7) lead to a cascade of coupled equations for the secular fields and higher harmonics. We will see in Sec. III that $A_y(t) E_x^L$ and $A_y \partial_x A_y$ will generate higher harmonics. We will concentrate on the second harmonic and show that it can decrease absorption for the parameters considered in this paper or to put it differently increase reflectivity. We will find that $A_y(t) E_x^L$ and $A_y \partial_x A_y$ are of different strengths and have very different characteristics versus angle of incidence. In the next section we will give an approximate but self-consistent solution of our model equations (5), (6), and (7).

III. APPROXIMATE SOLUTION OF THE MODEL EQUATIONS

An approximate solution of the equations (5), (6), and (7) is found by first neglecting the terms quadratic in the field A_y . We then obtain self-consistent first-order solutions E_{x1} and A_{y1} . In a second step we reintroduce the first-order approximations into Eqs. (5), (6), and (7) and calculate the dc fields E_{x0} and A_{y0} and the second harmonics E_{x2} and A_{y2} . As we can see from Fig. 1, obtained with the help of relativistic Vlasov simulations, the intensity of higher harmonics falls off rapidly in the high-temperature limit, so it is sufficient to consider only the second for the parameters investigated in this paper. In addition, to save effort we shall not renormalize the first-order solutions. With an incident p -polarized wave, we first obtain for E_{x1}^L and A_{y1} inside the plasma,^{10,13}

$$\begin{aligned} E_{x1}^L(x, t) \approx & \Re \{ \hat{E}_{x1}^L(\theta) e^{-i\omega t} [\Theta(x) e^{-x/l_e} - \Theta(-x) e^{x/l_e}] \}, \\ A_{y1}(x, t) \approx & \Re \{ \hat{A}_{y1}(\theta) e^{-i\omega t} [\Theta(x) e^{-x/l_s} + \Theta(-x) e^{x/l_s}] \}, \end{aligned} \quad (8)$$

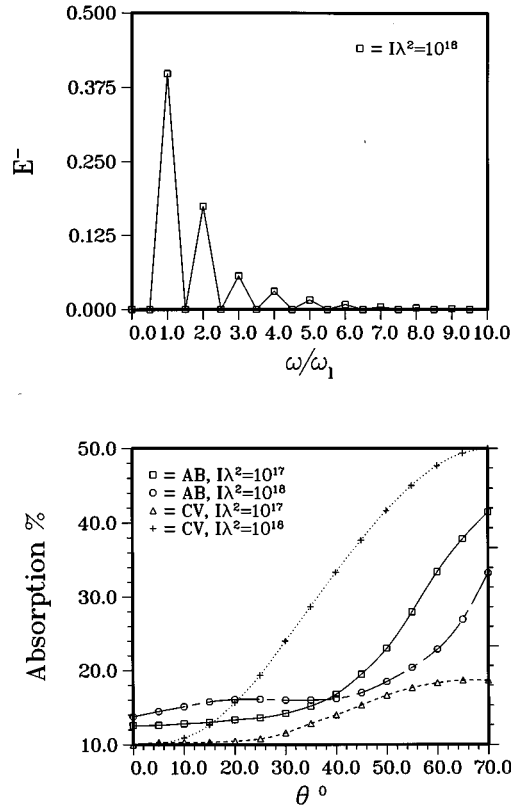


FIG. 1. Higher harmonics of the reflected light for $\theta=60^\circ$ and $I\lambda^2 = 10^{18} \text{ W cm}^{-2} \mu\text{m}^2$ (upper plot). AB (fractional absorption) and CE (fractional conversion efficiency) versus angle of incidence (lower plot). Both plots have been obtained by a Vlasov simulation for $n/n_e = 25$, $T_e = 10 \text{ keV}$, and $L/\lambda = 0.01$.

$$\begin{aligned} \hat{E}_{x1}^L(\theta) &= 2i\omega B_{z1}(0^+) F_{x1}^L(0), \\ l_e &\approx \frac{1}{7\pi^{1/6}} \left(\frac{v_{th}c^2}{\bar{\gamma}\omega_p^2} \right)^{1/3} \left(\frac{c\omega}{v_{th}\omega_p} \right)^{2/3}, \\ \hat{A}_{y1}(\theta) &= -2B_{z1}(0^+) F_{y1}(0), \quad l_s \approx \frac{1}{\pi^{1/6}} \left(\frac{v_{th}c^2}{\bar{\gamma}\omega_p^2} \right)^{1/3}, \end{aligned} \quad (9)$$

$$\begin{aligned} F_{x1}^L(0) &= \int_{-\infty}^{\infty} \frac{dq}{2\pi} \frac{g_{xy}(q,\omega) - \bar{\beta}c(q/\omega)g_{xx}(q,\omega)}{g_{xx}(q,\omega)g_{yy}(q,\omega) - g_{xy}^2(q,\omega)}, \\ F_{y1}(0) &= \int_{-\infty}^{\infty} \frac{dq}{2\pi} \frac{g_{xx}(q,\omega)}{g_{xx}(q,\omega)g_{yy}(q,\omega) - g_{xy}^2(q,\omega)}, \end{aligned} \quad (10)$$

$$\begin{aligned} g_{xx}(q,\omega) &= -\frac{\omega_p^2\omega}{c^2} \left(\frac{\bar{\gamma}^2\omega}{q^2v_{th}^2} [1+X(q,\omega)] + \frac{\omega}{\omega_p^2} \right), \\ g_{xy}(q,\omega) &= -\frac{\omega_p^2\omega}{c^2} \frac{\bar{\gamma}^2}{v_{th}^2} \bar{\beta}c [1+X(q,\omega)], \\ g_{yy}(q,\omega) &= -\frac{\omega_p^2\omega}{c^2} \left[\frac{\bar{\gamma}^2}{v_{th}^2\omega} \bar{\beta}^2c^2 [1+X(q,\omega)] \right. \\ &\quad \left. + \frac{1}{\omega\bar{\gamma}^2} X(q,\omega) + \frac{c^2}{\omega_p^2\omega} \left(\frac{\omega^2}{c^2} - q^2 \right) \right], \end{aligned} \quad (11)$$

and

$$X(q,\omega) = \frac{\bar{\gamma}\omega}{\sqrt{2v_{th}^2q^2}} Z \left(\bar{\gamma} \frac{\omega + i\nu}{\sqrt{2v_{th}^2q^2}} \right). \quad (12)$$

The function Z denotes the plasma dispersion function.¹⁶ The symmetry of the fields in Eqs. (8) is such as to reproduce, for straight line orbits, the effect of specular electron reflection. The different skin lengths l_s and l_e for the transverse and longitudinal fields give rise to the effects discussed earlier. Requiring continuity at the vacuum plasma interface yields for $B_{z1}(0^+)$,

$$B_{z1}(0^+) = \frac{2E_0}{c\bar{\gamma}} \frac{1+i(2\omega/c)F_{y1}(0)}{1-i(2\omega/c)F_{y1}(0)}. \quad (13)$$

We now insert Eqs. (8) into Eqs. (5) and (7) to obtain for E_{x0}^L ,

$$\begin{aligned} \bar{\gamma}E_{x0}^L(x) &= \left(\frac{e|\hat{A}_{y1}(\theta)|^2}{m\bar{\gamma}^2l_s} - \frac{e\Re[\hat{A}_{y1}^*(\theta)\hat{E}_{x1}^L(\theta)]}{mc} \right) \bar{\beta} \\ &\quad \times H_1(x, l_s, \lambda_D), \\ H_1(x, l_s, \lambda_D) &= \frac{1}{2(1-4\lambda_D^2/l_s^2)} [e^{-2x/l_s} - e^{-x/\lambda_D}], \end{aligned} \quad (14)$$

where $\lambda_D = v_{th}/\omega_p = (\omega v_{th}^2/\omega_p c^2) l_s$. Equation (14) demonstrates the effect of a force on the electrons in the direction of growing field strength of the oscillating fields due to the nonlocal light pressure term proportional to $\Re[\hat{A}_{y1}^*(\theta)\hat{E}_{x1}^L(\theta)]$. This force acts on the length scale $l_e \ll l_s$ and leads to a negative charge accumulation close to the vacuum-plasma boundary.¹⁷ The next step consists of calculating the second harmonics from the first-order solution of Eqs. (8). We obtain by introducing Eqs. (8) into Eqs. (5), (6), and (7) and Fourier transforming

$$\begin{aligned} \partial_t E_{x2} &= i\omega_p^2 e^{-2i\omega t} \int_{-\infty}^{\infty} \frac{dk}{2\pi} e^{-ikx} \\ &\quad \times \left(\bar{E}_{x2}^L + \frac{e\hat{A}_{y1}^2(\theta)}{im\bar{\gamma}^3 l_s} \frac{k}{k^2 + (4/l_s^2)} \right) \frac{2\bar{\gamma}^2\omega}{v_{th}^2 k^2} \\ &\quad \times [1 + X(k, 2\omega)] \end{aligned} \quad (15)$$

and

$$\begin{aligned} \left(\partial_x^2 - \frac{1}{c^2} \partial_t^2 \right) A_{y2} &= i \frac{\omega_p^2}{c^2} e^{-2i\omega t} \int_{-\infty}^{\infty} \frac{dk}{2\pi} e^{-ikx} \left[\frac{1}{\bar{\gamma}^2} X(k, 2\omega) i\bar{A}_{y2} \right. \\ &\quad \left. + \frac{\bar{\beta}\bar{\gamma}^2 c}{v_{th}^2 k} [1 + X(k, 2\omega)] \left(\bar{E}_{x2}^L + \frac{e\hat{A}_{y1}^2(\theta)}{im\bar{\gamma}^3 l_s} \frac{k}{k^2 + (4/l_s^2)} \right) \right. \\ &\quad \left. + \frac{\bar{\gamma}^2}{v_{th}^2 k} [1 + X(k, \omega)] \frac{e\hat{A}_{y1}(\theta)\hat{E}_{x1}^L(\theta)}{im\bar{\gamma}^3} \frac{\bar{k}}{\bar{k}^2 + (1/l_e^2)} \right], \end{aligned} \quad (16)$$

where $\bar{k} = k + i/l_s$. The quantities \bar{A}_y and \bar{E}_x^L denote the Fourier transforms of the fields A_y and E_x^L . The amplitude of the

second harmonic is now determined by requiring continuous solutions at the vacuum plasma boundary exactly in the same fashion as for the fundamental mode. As a consequence, the reflected light will contain the second harmonic in addition to the fundamental. The result for the amplitude of the second harmonic of the transverse field E_{y2} is

$$E_{y2}(x,t) = e^{-2i\omega t} [T_{y2}(x) + L_{y2}(x) - 4i\omega B_{z2}(0^+) F_{y2}(x)], \quad (17)$$

$$F_{y2}(x) = \int_{-\infty}^{\infty} \frac{dq}{2\pi} e^{-iqx} \times \frac{g_{xx}(q,2\omega)}{g_{xx}(q,2\omega)g_{yy}(q,2\omega) - g_{xy}^2(q,2\omega)},$$

$$L_{y2}(x) = -\frac{2eP_l}{im\omega\bar{\gamma}^3} \int_{-\infty}^{\infty} \frac{dq}{2\pi} e^{-iqx} \times \frac{q^2}{q^2 + 1/l_e^2} \frac{[g_{xx}(q,\omega) + (\omega^2/c^2)]g_{xx}(q,2\omega)}{g_{xx}(q,2\omega)g_{yy}(q,2\omega) - g_{xy}^2(q,2\omega)},$$

$$T_{y2}(x) = \frac{4e\omega^2 P_t}{imc^2\bar{\gamma}^3 l_s} \int_{-\infty}^{\infty} \frac{dq}{2\pi} e^{-iqx} \frac{q}{q^2 + 4/l_s^2} \times \frac{g_{xy}(q,2\omega)}{g_{xx}(q,2\omega)g_{yy}(q,2\omega) - g_{xy}^2(q,2\omega)},$$

$$B_{z2}(0^+) = \frac{1}{c} \frac{L_{y2}(0) + T_{y2}(0)}{1 - i(4\omega/c)F_{y2}(0)}. \quad (18)$$

The quantities $P_l = \hat{A}_{y1}(\theta)\hat{E}_{x1}^L(\theta)$ and $P_t = \hat{A}_{y1}^2(\theta)$ describe the self-coupling strengths of the transverse field A_y to longitudinal and transverse plasma oscillations [coupling terms $A_y(t)E_x^L$ and $A_y \partial_x A_y$]. It is interesting to note that L_{y2} dominates T_{y2} . Next we will give the analytical formula for fractional absorption (AB) that consists of the normalized incoming energy flux represented by 1 minus the emitted energy flux for the fundamental mode minus the emitted energy flux for the second harmonic. It is given by

$$T = 1 - \frac{1 - (4\omega/c)\Im F_{y1}(0) + (4\omega^2/c^2)}{1 + (4\omega/c)\Im F_{y1}(0) + (4\omega^2/c^2)|F_{y1}(0)|^2} - \frac{(\bar{\gamma}^2/E_0^2)|L_{y2}(0) + T_{y2}(0)|^2}{1 + (8\omega/c)\Im F_{y2}(0) + (16\omega^2/c^2)|F_{y2}(0)|^2}. \quad (19)$$

This formula has been obtained formally by demanding continuous solutions at the boundary and shows the additive property of fractional absorption in the high-temperature case considered here. We define the fractional conversion efficiency for the second harmonic (CE) as the ratio of the emitted intensity of the second harmonic to the irradiated intensity. It is given by the third term of Eq. (19). Since L_{y2} and T_{y2} scale like intensity CE scales like intensity while the absolute conversion scales like intensity squared. This is in agreement with measurements by Norreys *et al.*¹⁸

IV. VLASOV SIMULATION OF FRACTIONAL ABSORPTION

We consider a plasma slab that is inhomogeneous only in the x direction and completely homogeneous in all other directions. For agreement with the analytical model we assume a static ion background. The extension to account for ion motion is straightforward. A p -polarized laser pulse approximated by a plane wave is assumed to impinge the plasma under an arbitrary angle of incidence θ . A simple Lorentz transformation is then applied to reduce the two-dimensional (2-D) spatial geometry for oblique incidence to a one-dimensional (1-D) geometry for normal incidence (boost technique;¹¹ see Sec. II). The distribution function f_e is a Lorentz scalar. Then, in the boosted frame the electron distribution function $f_e(x, p_x, p_y, t)$ obeys the following relativistic Vlasov equation [in the following the index $e(i)$ refers to the electrons (ions)],

$$[\partial_t + v_{ex}\partial_x - e(E_x + v_{ey}B_z)\partial_{p_{ex}} - e(E_y - v_{ex}B_z)\partial_{p_{ey}}]f_e = 0, \quad (20)$$

where

$$v_{ex/y} = \frac{cp_{ex/y}}{\sqrt{m_e^2c^2 + p_{ex}^2 + p_{ey}^2}} \quad (21)$$

is the $x(y)$ electron velocity component. The longitudinal and transverse electromagnetic fields E_x , E_y , and B_z are given by Maxwell's equations,

$$\partial_x E_x = \frac{1}{\epsilon_0} \rho, \quad (22)$$

$$\partial_t E_x = -\frac{1}{\epsilon_0} j_x, \quad (23)$$

$$\partial_x E_y = -\partial_t B_z, \quad (24)$$

$$\partial_t E_y = -c^2 \partial_x B_z - \frac{1}{\epsilon_0} j_y, \quad (25)$$

where the charge and current densities ρ , j_x , and j_y are given by

$$\rho = -e \int_{-\infty}^{\infty} dp_{ex} \int_{-\infty}^{\infty} dp_{ey} f_e + Ze \int_{-\infty}^{\infty} dp_{ix} \int_{-\infty}^{\infty} dp_{iy} f_i,$$

$$j_x = -e \int_{-\infty}^{\infty} dp_{ex} \int_{-\infty}^{\infty} dp_{ey} v_{ex} f_e + Ze \int_{-\infty}^{\infty} dp_{ix} \int_{-\infty}^{\infty} dp_{iy} v_{ix} f_i,$$

$$j_y = -e \int_{-\infty}^{\infty} dp_{ex} \int_{-\infty}^{\infty} dp_{ey} v_{ey} f_e + Ze \int_{-\infty}^{\infty} dp_{ix} \int_{-\infty}^{\infty} dp_{iy} v_{iy} f_i. \quad (26)$$

Here Z is the charge state of the ions. Equations (22)–(25) can be rewritten in a conservational form more suitable for our numerical purposes,

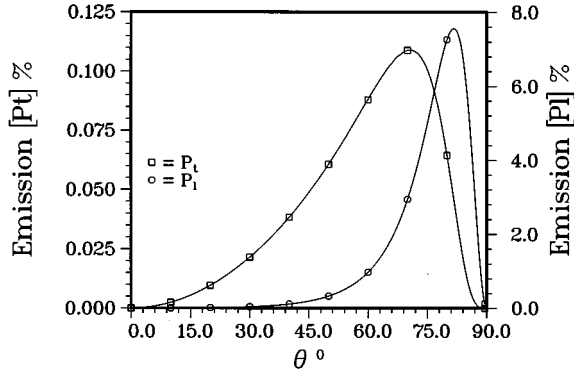
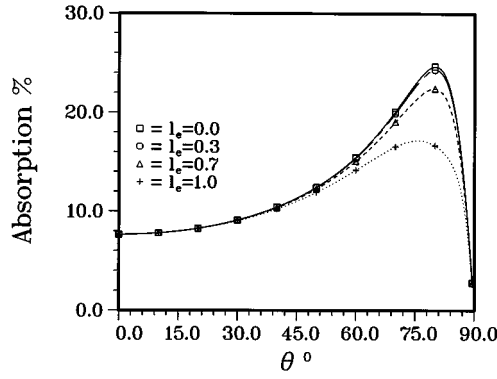


FIG. 2. AB versus angle of incidence. Coupling to longitudinal plasma oscillations turned off for $l_e = 0.0$ and turned on for $l_e = 1.0$ (upper plot). CE versus angle of incidence due to P_l and P_t (lower plot). Both plots have been obtained analytically for a step-like density profile. The parameters are $n/n_c = 25$, $T_e = 10$ keV, and $I\lambda^2 = 10^{18}$ W cm $^{-2}$ μm^2 .

$$\partial_t \mathcal{E}_x + \frac{j_x}{\rho + C} \partial_x \mathcal{E}_x = 0, \quad (27)$$

where $\mathcal{E}_x = E_x + Cx$, with $\rho + C > 0$, $C \gg 1$ being a constant introduced for numerical reasons (we choose $C \sim 10^3$). Furthermore, concerning the transverse part of Maxwell's equations, i.e. Eqs. (24) and (25), we write

$$(\partial_t \pm c \partial_x) E^\pm = -\frac{1}{\epsilon_0} j_y, \quad (28)$$

where $E^\pm = E_y \pm cB_z$. To fix the initial and boundary conditions for the electromagnetic fields and the electron distribution function f_e , we observe that Eqs. (20), (27), and (28) preserve their shape for an arbitrary angle of incidence θ if E_x , E^\pm and f_e are given, respectively, by

$$\begin{aligned} E^+(0, t) &= \frac{2}{\gamma} E_0 \sin \omega t, \\ E^-(\infty, t) &= 0, \\ E_x(x, 0) &= E^\pm(x, 0) = 0, \end{aligned} \quad (29)$$

and

$$\begin{aligned} f_e(x, p_{ex}, p_{ey}, 0) &= N_e n_e(x) \exp \left[-\frac{m_e c^2}{k_B T_e} \right. \\ &\quad \left. \times \left(\sqrt{1 + \frac{p_{ex}^2 + p_{ey}^2}{m_e^2 c^2}} - 1 \right) \right], \end{aligned} \quad (30)$$

where

$$h_e(p_{ex}, p_{ey}) = \bar{\gamma}(p_{ey} + \bar{\beta} \sqrt{m_e^2 c^2 + p_{ex}^2 + p_{ey}^2}) \quad (31)$$

and

$$\begin{aligned} N_e^{-1} &= \int_{-\infty}^{\infty} dp_{ex} \int_{-\infty}^{\infty} dp_{ey} \\ &\quad \times \exp \left[-\frac{m_e c^2}{k_B T_e} \left(\sqrt{1 + \frac{p_{ex}^2 + p_{ey}^2}{m_e^2 c^2}} - 1 \right) \right]. \end{aligned} \quad (32)$$

Equation (30) is obtained assuming that $f_e(0)$ is Maxwellian and requiring that f_e transforms like a scalar. The details of an efficient fully relativistic numerical scheme for integrating Eqs. (20), (22)–(25) are beyond the scope of this paper.

The size of the simulation box is 6λ for $x(0 \leq x \leq 6\lambda)$, where λ is the vacuum wavelength of the laser light and $80m v_{th}$ for p_x and p_y . The component p_z is not needed for the pure p -polarization case (see Sec. II). Since it is necessary to resolve scale lengths of the order of a thermal Debye length (see Sec. III), the spatial resolution has been chosen to be $0.5\lambda_D = 0.5v_{th}/\omega_p$. In momentum space we choose $0.2m v_{th}$. The position of the vacuum plasma interface is located at $x = 2\lambda$. Those electrons that reach the boundaries are allowed to escape. No electrons enter at the vacuum boundary located at $x = 0$. At $x = 6\lambda$ thermal electrons with the initial temperature are allowed to enter. We do not choose a step-like density profile but a very small finite scale length ($L/\lambda = 0.01$). The temperature of the simulations is $T_e = 10$ keV and the density $n/n_c = 25$. For these parameters we obtain $l_s \approx 6.3\lambda_D = 1.26v_{th}/\omega$, $l_e \approx 1.1\lambda_D = 0.23v_{th}/\omega$, and $\lambda_D = 0.0045\lambda$.

The first plot of Fig. 1 shows the amplitudes of the higher harmonics normalized onto the amplitude of the incident radiation obtained by a Vlasov simulation for $T_e = 10$ keV and $I\lambda^2 = 10^{18}$ W cm $^{-2}$ μm^2 . We observe that the spectrum of the emitted higher harmonics goes up to the ninth order. The second plot of Fig. 1 gives AB and CE for the same temperature and for $I\lambda^2 = 10^{17}$ W cm $^{-2}$ μm^2 and $I\lambda^2 = 10^{18}$ W cm $^{-2}$ μm^2 . It shows a decrease of AB for growing intensity.^{5,8} The magnitude of AB for $\theta = 60^\circ$ and $I\lambda^2 = 10^{18}$ W cm $^{-2}$ μm^2 can be determined from the spectrum given in the first plot of Fig. 1. The outgoing energy flux contained in the fundamental mode plus the second harmonic already gives a good approximation for the observed AB. This result verifies the additive character of AB given by Eq. (19) for the parameters considered here. The maximum CE for $I\lambda^2 = 10^{17}$ W cm $^{-2}$ μm^2 is about 3% while it is almost 12% for $I\lambda^2 = 10^{18}$ W cm $^{-2}$ μm^2 . In addition, we

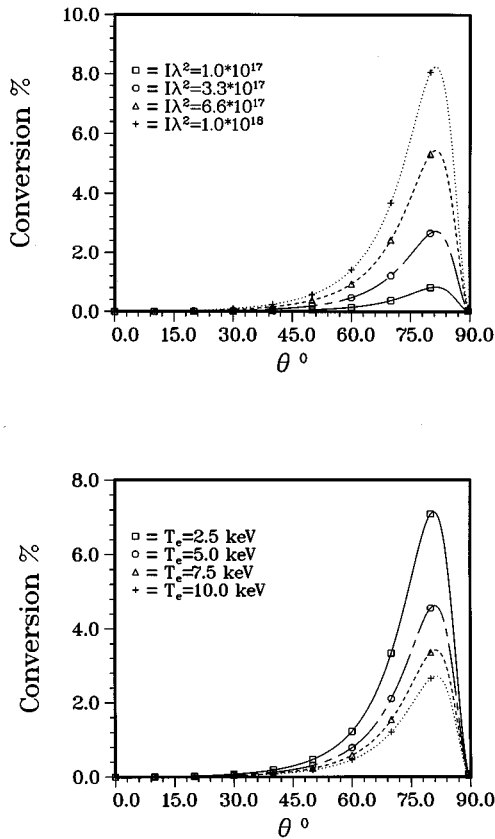


FIG. 3. CE for various irradiances (upper plot) and various temperatures (lower plot) versus angle of incidence. The parameters are $n/n_c = 25$ and $T_e = 10$ keV (upper plot) and $n/n_c = 25$ and $I\lambda^2 = 3.3 \times 10^{17}$ W cm $^{-2}$ μm^2 (lower plot).

find that AB is only weakly sensitive to intensity for normal incidence, as expected from the discussion above.

V. DISCUSSION AND SUMMARY

As we can see from the second plot of Fig. 1 that was obtained by a Vlasov simulation AB decreases with growing irradiation. The same result is obtained analytically (see Fig. 2). The upper plot of Fig. 2 gives AB for various coupling strengths (indicated by l_e) to longitudinal plasma oscillations. If we consider the normalized skin length l_e as a formal coupling parameter we can turn on and off the coupling of the laser light to the surface oscillations discussed in Sec. II ($l_e = 0.0$ means no coupling, $l_e = 1.0$ means full coupling). The lower plot of Fig. 2 gives the analytical results of fractional emission of the second harmonic due to P_1 and P_t for a step-like density profile ($P_1 \gg P_t$). Figures 3 and 4 show CE for various irradiancies, temperatures, and densities. Our model predicts that fractional conversion grows linearly with intensity (this means that conversion grows as intensity squared), which is in agreement with experiments.¹⁸ However, we note that we did not renormalize the first-order solution given by Eq. (8). In addition, since electron uphill acceleration provides a shielding process we expect enhanced target surface expansion, which should be included in future calculations.¹⁷ From the lower plot of Fig. 3 we see that growing temperatures reduce CE. This result indicates

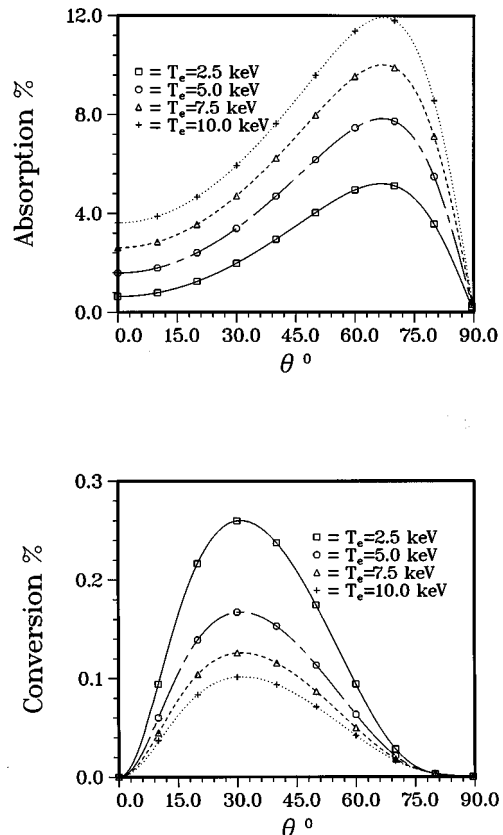


FIG. 4. AB (upper plot) and CE (lower plot) for various temperatures versus angle of incidence for $n/n_c = 4.4$ and $I\lambda^2 = 3.3 \times 10^{17}$ W cm $^{-2}$ μm^2 .

that low temperatures are necessary for high-order harmonics. For the parameters of Fig. 2 we obtain $\omega_p v_{os}^2 / \omega c v_{th} \approx 18$. The results still agree well with the numerical data. Thus, we conclude that the formal restriction given in Sec. II is not severe and can be extended up to 18. This is due to the fact that in the overdense plasma the amplitudes are much smaller than the vacuum amplitudes, which have been assumed to derive the criterion of Sec. II. The upper plot of Fig. 4 gives AB for $n/n_c = 4.4$. For this density that is close to the critical density for the second harmonic, the analytical model predicts almost no conversion, a result we consider being reasonable. In addition, the optimum conversion angle drops to $\theta \approx 30^\circ$.

We conclude as follows. The second harmonic emission is able to reduce fractional absorption considerably for high temperatures. This process might also play a role for lower temperatures, where our approximations become questionable. The coupling of the transverse field to longitudinal plasma oscillations (coupling parameter P_1) provides the dominant mechanism of harmonics generation for step-like density profiles supporting the hypothesis of Lichters *et al.*¹⁵ while the coupling to transverse plasma oscillations (coupling parameter P_t) is less effective in that case. However, this second coupling mechanism may play a role for finite density gradients.

ACKNOWLEDGMENTS

This work was partially supported by the European Commission through the TMR network SILASI (Super In-

tense LAser-pulse Solid Interaction), Contract No. ERBFMRX-CT96-0043. One of the authors (R.A.C.) was also supported by EPSRC Grant No. GR/K58937.

¹H. M. Milchberg and R. R. Freeman, *Phys. Fluids* **2**, 1395 (1990).

²U. Teubener, J. Bergmann, B. van Wousterghem, F. P. Schäfer, and R. Sauerbrey, *Phys. Rev. Lett.* **70**, 794 (1993).

³D. F. Price, R. M. More, R. S. Walling, G. Guethlein, R. L. Shepherd, R. E. Stewart, and W. E. White, *Phys. Rev. Lett.* **75**, 252 (1995).

⁴W. Rozmus, R. Cauble, and V. T. Tikhonchuk, *Phys. Plasmas* **3**, 360 (1996).

⁵P. Gibbon and A. R. Bell, *Phys. Rev. Lett.* **68**, 1535 (1992).

⁶P. Gibbon, *Phys. Rev. Lett.* **73**, 664 (1994).

⁷P. Gibbon, *Phys. Rev. Lett.* **76**, 50 (1996).

⁸H. Ruhl and P. Mulser, *Phys. Lett. A* **205**, 388 (1995).

⁹T.-Y. B. Yang, W. L. Kruer, A. B. Langdon, and T. W. Johnston, *Phys. Plasmas* **3**, 2702 (1996).

¹⁰H. Ruhl, *J. Opt. Soc. Am. B* **13**, 388 (1996).

¹¹A. Bourdier, *Phys. Fluids* **26**, 1804 (1983).

¹²F. Brunel, *Phys. Rev. Lett.* **59**, 52 (1987).

¹³A. A. Andreev, E. G. Gamalii, V. N. Novikov, A. N. Semakhin, and V. T. Tikhonchuk, *Sov. Phys. JETP* **74**, 963 (1992).

¹⁴N. S. Erokin, V. E. Zakharov, and S. S. Moissev, *Sov. Phys. JETP* **29**, 101 (1969).

¹⁵R. Lichters, J. Meyer-ter-Vehn, and A. Pukhov, *Phys. Plasmas* **3**, 3425 (1996).

¹⁶B. D. Fried and S. D. Conte, *The Plasma Dispersion Function* (Academic, New York, 1961), p. 1.

¹⁷H. Ruhl, *Phys. Plasmas* **3**, 3129 (1996).

¹⁸P. A. Norreys, M. Zepf, S. Moustazis, A. P. Fews, J. Zhang, P. Lee, M. Bakarezos, C. N. Danson, A. Dyson, P. Gibbon, P. Loukakos, D. Neely, F. N. Walsh, J. S. Wark, and A. E. Dangor, *Phys. Rev. Lett.* **76**, 1832 (1996).